Structural and functional insight into regulation of kinesin-1 by microtubule-associated protein MAP7

Ferro, Luke S.; Fang, Qianglin; Eshun-Wilson, Lisa; Fernandes, Jonathan; Jack, Amanda; Farrell, Daniel P.; Golcuk, Mert; Huijben, Teun; Costa, Katelyn; More Authors

DOI
10.1126/science.abf6154

Publication date
2022

Document Version
Final published version

Published in
Science

MOLECULAR MOTORS

Structural and functional insight into regulation of kinesin-1 by microtubule-associated protein MAP7

Luke S. Ferro[1]†, Qianglin Fang[1]*†‡, Lisa Eshun-Wilson[1]†, Jonathan Fernandes[2]†, Amanda Jack[3], Daniel P. Farrell[4], Mert Golcuk[5], Teun Huijben[6], Katelyn Costa[7], Mert Gur[5], Frank DiMaio[4], Eva Nogales[1,3,8,9]*, Ahmet Yildiz[1,3,9,10]*

Microtubule (MT)–associated protein 7 (MAP7) is a required cofactor for kinesin-1–driven transport of intracellular cargoes. Using cryo–electron microscopy and single–molecule imaging, we investigated how MAP7 binds MTs and facilitates kinesin-1 motility. The MT-binding domain (MTBD) of MAP7 bound MTs as an extended α helix between the protofilament ridge and the site of lateral contact. Unexpectedly, the MTBD partially overlapped with the binding site of kinesin-1 and inhibited its motility. However, by tethering kinesin-1 to the MT, the projection domain of MAP7 prevented dissociation of the motor and facilitated its binding to available neighboring sites. The inhibitory effect of the MTBD dominated as MTs became saturated with MAP7. Our results reveal biphasic regulation of kinesin-1 by MAP7 in the context of their competitive binding to MTs.

Kinesin and dynein are molecular motors that deliver intracellular cargos by walking along microtubules (MTs) (*1*, *2*). Intracellular cargos are differentially regulated by structural MT-associated proteins (MAPs) that decorate the MT surface (*1*). Distinct cellular localizations of MAPs correlate with their regulatory roles in intracellular traffic (*3*). Overexpression of tau disrupts kinesin-1 (hereafter kinesin)–driven transport of synaptic vesicles in axons (*4*, *5*), whereas the knockdown of tau rescues defects in axonal transport in Alzheimer's disease models (*6*). Unlike tau, MAP7 is a required cofactor for kinesin-driven transport in cells (*7*–*9*). The MAP7 projection domain binds to kinesin's coiled-coil stalk in vitro (*9*, *10*), recruits kinesin to MTs, and activates its motility (*9*, *11*). Transient interactions with the MAP7 projection domain may enable kinesin to hop from one MAP to another, increasing its apparent run length by disfavoring detachment from the MT (*9*).

To understand how MAP7 regulates kinesin, we determined the cryo–electron microscopy (cryo-EM) structure of MTs decorated with full-length (FL) MAP7 (Fig. 1, A and B; fig. S1A; tables S1 and S2; and movie S1). The reconstruction revealed a 53-residue-long α helix that runs parallel to the MT axis about the length of a tubulin dimer (Fig. 1, A to C, and fig. S1B). Unlike MAP2, MAP4, and tau, which bind along the outer ridges of the protofilaments (*12*–*14*), MAP7 runs halfway between the outer ridge and the site of lateral contact. The costructure of MAP7's MT binding domain (MTBD; residues 60 to 170) and FL tau on the MT (fig. S2) illustrated their distinct MT footprints and confirmed that the helical segment corresponds to the MTBD of MAP7. We identified a single MAP7 sequence register that corresponds to a well-conserved segment of the MTBD (residues 87 to 139; fig. S3, A to C) through Rosetta modeling (*15*) and validated this registry by determining the structure of MTs decorated with a shorter MAP7 construct (residues 83 to 134; fig. S3D). Because MAP7 MTBD could potentially form a helix longer than the length of a tubulin heterodimer (fig. S2A), we cannot exclude the possibility of a larger footprint of MAP7 on the MT (*13*) (fig. S4; see materials and methods).

The α-helical density for MAP7 is not uniform (Fig. 1B). Segment I (residues 113 to 139)—the best-resolved region (Fig. 1B)—interacts extensively with tubulin (Fig. 1D); Q113 and E117 of MAP7 are within hydrogen-bonding distance of N197 and S155 of β-tubulin, respectively; R114 and K127 of MAP7 engage in electrostatic interactions with E159 and D414 of β-tubulin, respectively. Y108 of β-tubulin inserts into a hydrophobic pocket formed by R120, R121, and V124 of MAP7. We also identified potential hydrogen bonds between R128, R131, and K136 of MAP7 and the mainchain oxygens of E411 and G410 of β-tubulin and V159 of α-tubulin, respectively. Segment III (residues 87 to 99) interacts with α-tubulin. Segment II (residues 100 to 113) faces a cavity at the intratubulin dimer and has the weakest density in our map (Fig. 1B). All-atom molecular dynamics (MD) simulations verified these pairwise interactions, and identified additional potential interactions between MAP7 and tubulin (fig. S5 and movie S2). Segment II fluctuated more than other segments in simulations because it only makes transient contacts with tubulin (Fig. 1, E and F, and fig. S5), explaining why this segment has weak density in our cryo-EM map.

We next determined how MAP7 affects the motility of kinesin and the dynein-dynactin-BicDR1 complex [(DDR), hereafter dynein] (*16*) (Fig. 2A). FL MAP7 uniformly decorated MTs with a dissociation constant (K_D) of 111 ± 12 nM (±SE) under physiological salt (Fig. 2, B and C, and fig. S6). As previously reported (*9*, *11*), the addition of 50-nM MAP7 rescued FL kinesin from autoinhibition (*17*) and substantially increased its run frequency and length (fig. S7). MAP7 also enhanced the motility of constitutively active kinesin (K560, residues 1 to 560) (Fig. 2, D and E and movie S3) (*9*, *11*). Unlike run length and frequency, kinesin velocity decreases even at low MAP7 concentrations (Fig. 2E), which could be a result of pausing at MTBD obstacles or binding to the projection domain. Previously, dynein has been reported not to be inhibited by 5-nM MAP7 (*10*); however, we found that it was inhibited by MAP7 with a half-maximal inhibition constant (IC_{50}) of 10 ± 3 nM (Fig. 2, D and E). MAP7 decoration of MTs also switched the direction of an assembly that links FL kinesin to dynein (Fig. 2F) (*18*). 80% of kinesin-dynein assemblies were minus-end–directed on undecorated MTs, whereas 93% moved toward the plus end upon addition of 10 nM MAP7 (Fig. 2, G and H, fig. S6C, and movie S4).

Unexpectedly, kinesin run frequency started to decrease when MAP7 concentration was increased further (100 to 1000 nM; Fig. 2, D and E, and movie S3). We reasoned that the nonlinear relationship between MAP7 decoration and kinesin motility could arise when the motor is subjected to simultaneous activation and inhibition that dominate at different concentrations (Fig. 2E) (*19*). To determine the source of these opposing inputs, we disrupted the kinesin-MAP7 interaction by truncating either the MAP7-binding domain of kinesin (K490, residues 1 to 490) or the kinesin-binding domain of MAP7 (MAP7-N and MAP7-MTBD; Fig. 3A). In all cases, MAP7 inhibited kinesin (Fig. 3B, fig. S8, and movies S5 and S6) as strongly as it inhibited dynein (Fig. 2E). Thus, MTBD inhibits whereas the projection domain activates kinesin (*10*).

MTBD may inhibit kinesin by competing for the same tubulin binding site, because superimposing the MT-bound structure of kinesin (*20*) onto our model reveals an apparent clash between kinesin and segment II of MAP7 (fig. S9A). Alternatively, the flexible segment II may accommodate kinesin binding by shifting away from the intradimer interface, as proposed for DCX and MAP4 (*14*, *21*).

[1]Department of Molecular and Cell Biology, University of California, Berkeley, CA, USA. [2]Department of Chemistry, University of California, Berkeley, CA, USA. [3]Biophysics Graduate Group, University of California, Berkeley, CA, USA. [4]Department of Biochemistry, University of Washington, Seattle, WA, USA. [5]Department of Mechanical Engineering, Istanbul Technical University, Istanbul, Turkey. [6]Department of Imaging Physics, Delft University of Technology, Delft, Netherlands. [7]Press West Illustrations, Boston, MA, USA. [8]Howard Hughes Medical Institute, University of California, Berkeley, CA, USA. [9]Molecular Biophysics and Integrative Bioimaging Division, Lawrence Berkeley National Laboratory, Berkeley, CA, USA. [10]Physics Department, University of California, Berkeley, CA, USA.
***Corresponding authors. yildiz@berkeley.edu (A.Y.); enogales@lbl.gov (E.N.); qfang168@berkeley.edu (Q.F.)**
†These authors contributed equally to this work.
‡Present address: School of Public Health, Sun Yat-sen University, Shenzhen, China.

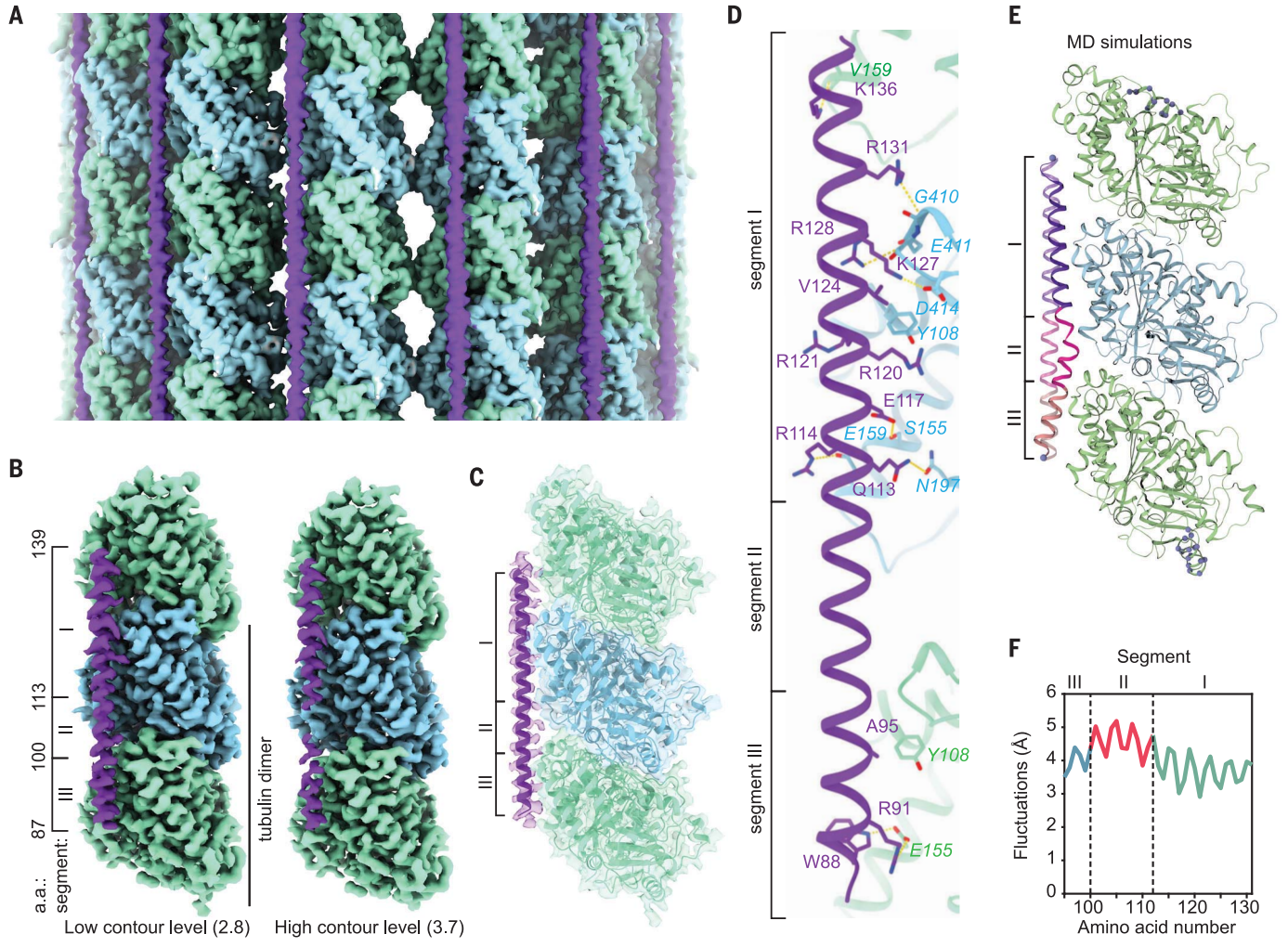

Fig. 1. MAP7 binds the MT between the outer protofilament ridge and the site of lateral contact. (**A**) Cryo-EM map (without symmetry expansion) of an MT decorated with MAP7; α-tubulin, β-tubulin, and MAP7 are shown in green, blue, and purple, respectively. (**B**) Improved MAP7-MT cryo-EM map after symmetry expansion and protofilament-based density subtraction (see methods). MAP7 binds across both inter- and intradimer interfaces. Weaker density is seen for the region over the intradimer interface (segment II), indicative of more flexibility and weaker interaction. Only one repeat of MAP7 and its neighboring tubulins are shown for clarity. a.a., amino acids. (**C**) Ribbon diagram for MAP7 and tubulin with the improved cryo-EM density map shown in gray. (**D**) Details of the interacting residues between MAP7 and its neighboring tubulins. Tubulin residues are shown in italics. (**E**) Initial and final MAP7-tubulin conformations obtained from an example all-atom MD simulation. Beads represent constrained atoms in MAP7 and tubulin. (**F**) Average root mean squared fluctuations of MAP7 Cα atoms from the cryo-EM structure coordinates within 200 ns (n = 4 simulations). Single-letter abbreviations for the amino acid residues are as follows: A, Ala; C, Cys; D, Asp; E, Glu; F, Phe; G, Gly; H, His; I, Ile; K, Lys; L, Leu; M, Met; N, Asn; P, Pro; Q, Gln; R, Arg; S, Ser; T, Thr; V, Val; W, Trp; and Y, Tyr.

To distinguish between these possibilities, we determined the structure of MTs incubated with rigor kinesin [K350, residues 1 to 350, E236A mutation (K350 ^{E236A})] and MAP7 (Fig. 3C). Because distinct binding sites of MAP7 and kinesin can be artifactually averaged during reconstruction (fig. S9B), we performed focused 3D classification around the putative shared binding site of MAP7 and kinesin (fig. S10; see methods). The classification resulted in two distinct maps of the binding site, one occupied by MAP7 only, and the other occupied by kinesin only (Fig. 3D). Thus, kinesin and MAP7 cannot simultaneously bind to the same tubulin dimer.

Consistent with cryo-EM, MTBD was unable to bind MTs predecorated with K350^{E236A} (Fig. 3E). However, FL MAP7 or a construct lacking the MTBD (ΔMTBD; fig. S11, A to C) still bound to K350^{E236A}-decorated MTs, presumably through the P123 domain (residues 175 to 316) (*8*, *9*). MT binding of ΔMTBD was nearly abolished upon cleaving the flexible tails of tubulin (Fig. 3E and fig. S11D), explaining why P123 was invisible in our structure. To verify that kinesin is inhibited at high levels of MAP7 decoration as a result of binding site overlap, we also replaced the MT-binding regions of MAP7 with that of tau, which also overlaps with the tubulin binding site of kinesin and inhibits kinesin motility (fig. S12) (*13*, *22*). Similar to FL MAP7, binding of this chimeric MAP to the MT resulted in biphasic regulation of kinesin motility (Fig. 3, F and G).

To reveal how kinesin "walks" along MAP7-decorated MTs despite competing for the same binding site, we fluorescently labeled the motor domain of K560 and tracked kinesin stepping with nanometer precision under limiting adenosine triphosphate (ATP) conditions (Fig. 4A). On undecorated MTs, kinesin took 16-nm steps in the forward direction (*23*), whereas steps

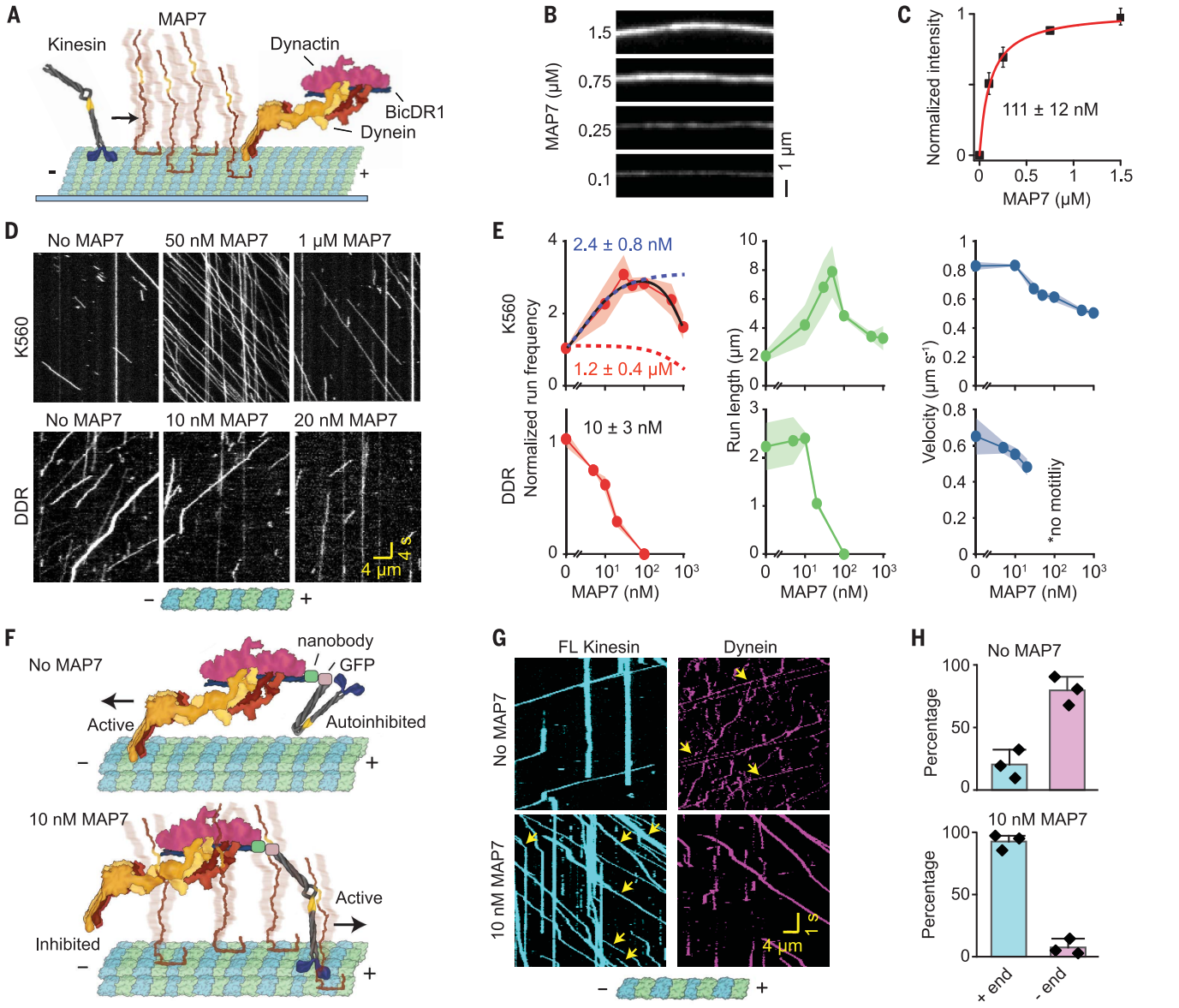

Fig. 2. MAP7 differentially regulates kinesin and dynein motility. (**A**) Schematic of kinesin and dynein motility on MTs coated with MAP7. (**B**) MT decoration of fluorescently labeled MAP7 under different concentrations. (**C**) Fluorescence intensity (mean ± SD) of MAP7 was fit to the Langmuir isotherm (solid curve) to calculate K_D (± SE). From left to right, n = 40, 44, 50, 68, and 109 MTs (two technical replicates). (**D**) Kymographs of K560 and dynein motility in the presence of MAP7. Assays were performed in 150 mM potassium acetate (KAc) and 0.1% methylcellulose. (**E**) Run frequency, run length, and velocity of K560 and dynein at different MAP7 concentrations (mean ± SEM). K560 run frequency was fit to the biphasic Hill equation (solid black curve) to reveal the half-maximal activation (blue dashed curve) and inhibition (red dashed curve) concentrations (± SE). Dynein run frequency was fit to the Langmuir equation (not shown) to calculate IC_{50} (± SE). From left to right, n = 281, 463, 532, 836, 381, and 433, and 233 for K560, and 386, 235, 213, and 146 for dynein; two technical replicates). (**F**) Schematic of kinesin and dynein assembled onto BicDR1. The addition of MAP7 switches the active motor. (**G**) Kymographs of kinesin-dynein assemblies with and without 10 nM MAP7. Yellow arrows show kinesin-dynein colocalizers. (**H**) Directionality of kinesin-dynein assemblies (mean ± SD, n = 356 and 580 for 0- and 10 nM MAP7, respectively, three replicates).

in the sideways and backward directions were rare (9 and 3%, respectively; Fig. 4, A and B, and fig. S13A) (*24*). At 36 nM MAP7, we observed a modest increase in the probability of sideways and backward stepping (Fig. 4, A and B). At nearly saturating MAP7 concentrations, we observed 16- to 64-nm displacements in our trajectories, as well as increased stepping in sideways (35%) and backward (26%) directions (Fig. 4, A and B). Because kinesin cannot take such large steps on its own (Fig. 4, A and B), these large displacements likely represent transient detachment and reattachment of the motor to the MT.

In the absence of the projection domain, kinesin was stuck on MTs decorated with 36-nM MTBD and dissociated from MTs at increased ATP concentrations (fig. S13, B and C). Furthermore, the addition of the C-terminal half of MAP7 (MAP7-C) was unable to stimulate kinesin motility on MTs decorated with the N-terminal half of MAP7 (MAP7-N, fig. S14). Thus, the projection domain is needed to be tethered to the MTBD to enable to bypass MTBD obstacles.

On the basis of our results and previous reports (*9*, *11*), we propose a model for kinesin

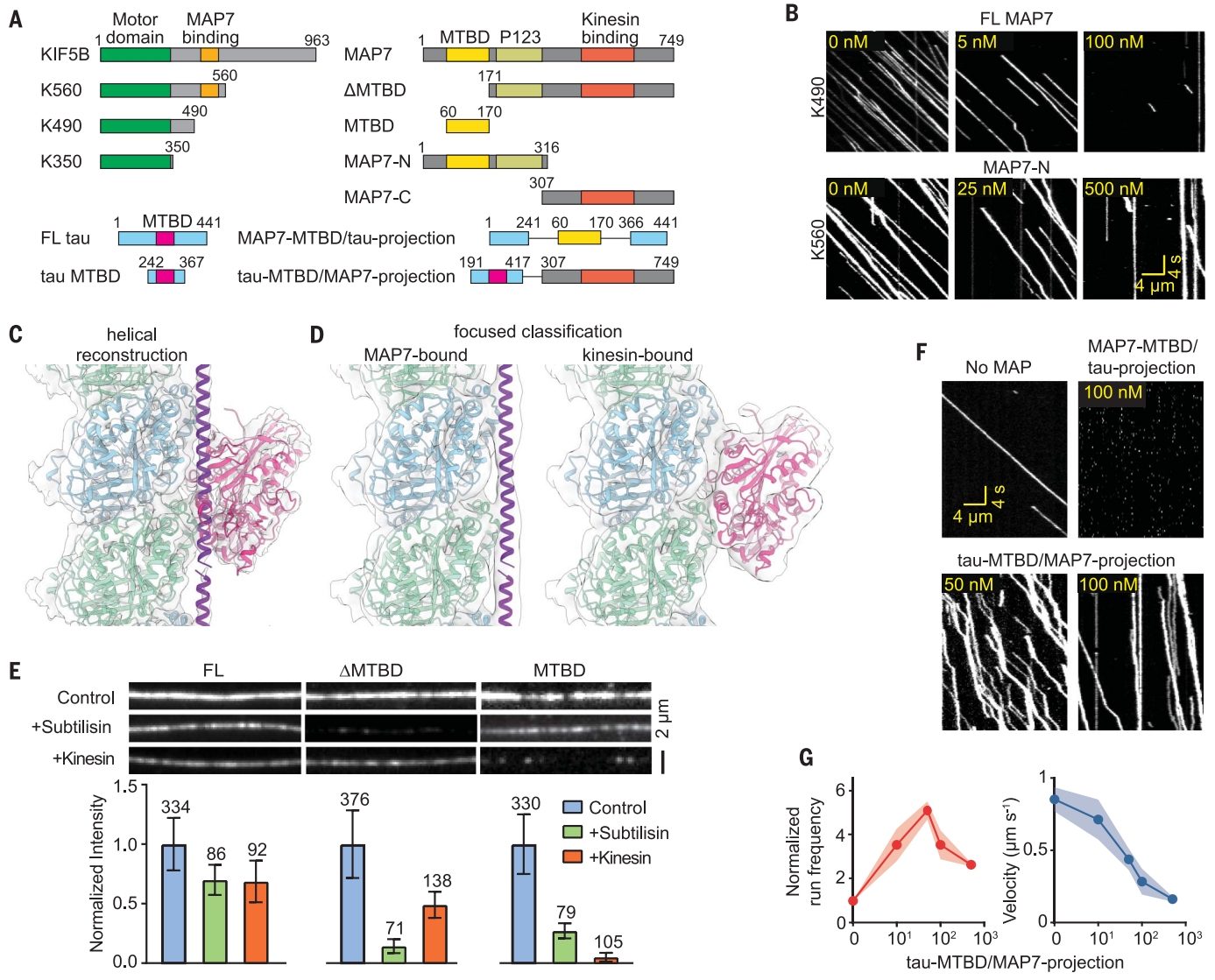

Fig. 3. MT tethering enables kinesin to move on MAP7-decorated MTs despite their overlapping binding sites. (**A**) Schematic of kinesin, MAP7, and tau constructs. (**B**) Kymographs showing kinesin motility in the presence of FL and truncated MAP7. (**C**) Average cryo-EM map of an MT decorated with both MAP7 and rigor kinesin. Atomic model of MAP7 and previously reported structure of kinesin on MT (PDB code: 4HNA) (*20*) were fitted into the cryo-EM map. (**D**) Focused 3D classification resulted in two distinct density maps showing either MAP7-bound (left) or kinesin-bound (right) tubulin, indicating competitive binding. (**E**) Fluorescent signal (top) and normalized intensity (bottom) of 1 μM LD655-labeled MAP7 constructs on MTs that are either untreated (control), subtilisin-treated, or predecorated with 1 μM rigor kinesin (mean ± SEM; *n* values are given for each bar). (**F**) Kinesin motility in the presence of chimeric MAPs. (**G**) Run frequency and velocity of kinesin in the presence of Tau-MTBD/MAP7-projection (mean ± SEM, *n* = 27, 112, 211, 102, and 55 from left to right, two technical replicates).

stepping on MAP7-decorated MTs. MAP7 recruits kinesin-1 to the MT and activates subsequent motility (*9*, *11*). MT binding of MAP7 also obstructs kinesin stepping along the protofilament, which results in kinesin dissociation from the MT. However, the MAP7 projection domain tethers kinesin to the MT surface, allowing it to rebind the MT at nearby sites not blocked by its MTBD. This "tethered diffusion" of kinesin appears as large forward, sideways, or backward displacements in our trajectories. When the MT surface is nearly saturated with MAP7, the frequency and length of kinesin runs are reduced because of the scarcity of empty tubulin sites to which the motor can rebind after it dissociates (Fig. 4C). Unlike kinesin-1, MAP7 inhibits dynein motility because its MTBD overlaps with the dynein binding site (fig. S15) but its projection domain does not tether dynein to MTs.

This biphasic regulation mechanism may enable precise control of kinesin-1–driven transport by varying MAP7 density on cellular MTs. Although MAP7 is required for kinesin-1-driven processes in many cell types (*10*, *25*, *26*), dense MAP7 localization was shown to slow and pause organelle transport at brunch junctions in rat neurons (*8*). Increased accumulation of MAP7 may reroute cargos to their destinations by facilitating the detachment of kinesin from its MT track and rebinding to neighboring MTs at these junctions (*8*).

REFERENCES AND NOTES

1. S. Bodakuntla, A. S. Jijumon, C. Villablanca, C. Gonzalez-Billault, C. Janke, *Trends Cell Biol.* **29**, 804–819 (2019).
2. A. Roll-Mecak, *Dev. Cell* **54**, 7–20 (2020).
3. L. F. Gumy *et al.*, *Neuron* **94**, 347–362.e7 (2017).
4. A. Ebneth *et al.*, *J. Cell Biol.* **143**, 777–794 (1998).
5. T. Ishihara *et al.*, *Neuron* **24**, 751–762 (1999).
6. K. A. Vossel *et al.*, *Science* **330**, 198 (2010).

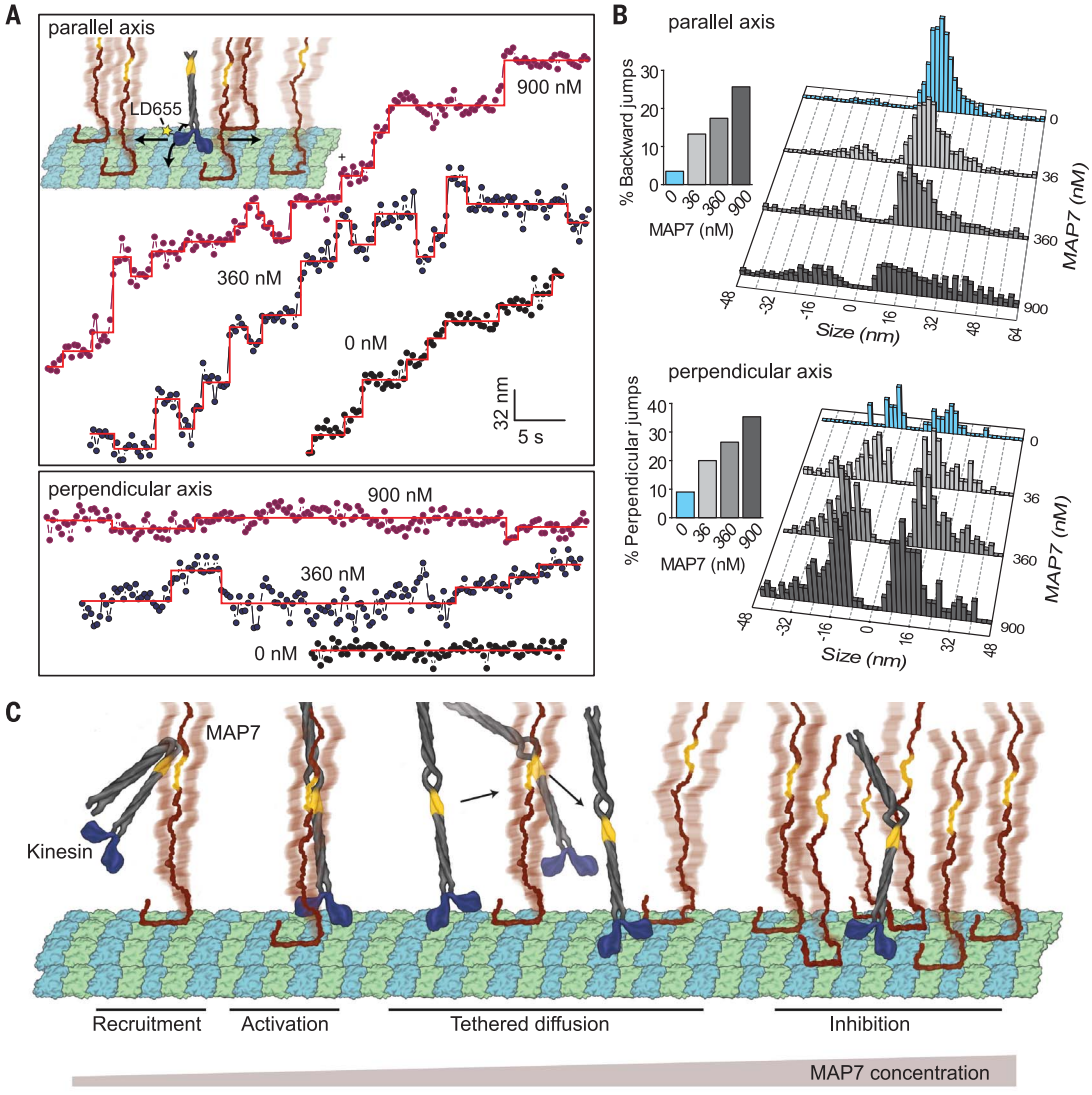

Fig. 4. Kinesin bypasses MTBD obstacles through tethered diffusion. (**A**) (Inset) K560 was labeled with LD655 at its N terminus, and its stepping was tracked in parallel (straight arrows) and perpendicular (curved arrows) axes of MTs under different MAP7 concentrations. Representative traces of K560 motility along parallel (top) and perpendicular (bottom) directions. Horizontal lines represent a fit to a step-finding algorithm. (**B**) Histograms reveal the percentage of instantaneous jumps in backward and perpendicular directions under different MAP7 concentrations (bar graphs). From top to bottom, n = 437, 580, 502, and 331 for parallel and 43, 145, 195, and 181 for perpendicular directions. (**C**) Model for regulation of kinesin by MAP7. The MAP7 projection domain rescues kinesin from autoinhibition and tethers the motor to the MT. When kinesin encounters an MTBD obstacle, it dissociates from the MT, remains tethered to MAP7, and rebinds to an available tubulin site on another protofilament. Kinesin is inhibited at high MAP7 concentrations due to the scarcity of available binding sites.

7. K. Barlan, W. Lu, V. I. Gelfand, *Curr. Biol.* **23**, 317–322 (2013).
8. S. R. Tymanskyj, B. H. Yang, K. J. Verhey, L. Ma, *eLife* **7**, e36374 (2018).
9. P. J. Hooikaas *et al.*, *J. Cell Biol.* **218**, 1298–1318 (2019).
10. B. Y. Monroy *et al.*, *Nat. Commun.* **9**, 1487 (2018).
11. B. Y. Monroy *et al.*, *Dev. Cell* **53**, 60–72.e4 (2020).
12. J. Al-Bassam, R. S. Ozer, D. Safer, S. Halpain, R. A. Milligan, *J. Cell Biol.* **157**, 1187–1196 (2002).
13. E. H. Kellogg *et al.*, *Science* **360**, 1242–1246 (2018).
14. H. Shigematsu *et al.*, *J. Cell Biol.* **217**, 4155–4163 (2018).
15. Y. Song *et al.*, *Structure* **21**, 1735–1742 (2013).
16. J. T. Canty, R. Tan, E. Kusakci, J. Fernandes, A. Yildiz, *Annu. Rev. Biophys.* **50**, 549–574 (2021).
17. K. J. Verhey, N. Kaul, V. Soppina, *Annu. Rev. Biophys.* **40**, 267–288 (2011).
18. A. R. Chaudhary *et al.*, *J. Biol. Chem.* **294**, 10160–10171 (2019).
19. M. L. Valenstein, A. Roll-Mecak, *Cell* **164**, 911–921 (2016).
20. B. Gigant *et al.*, *Nat. Struct. Mol. Biol.* **20**, 1001–1007 (2013).
21. J. S. Liu *et al.*, *Mol. Cell* **47**, 707–721 (2012).
22. R. Dixit, J. L. Ross, Y. E. Goldman, E. L. Holzbaur, *Science* **319**, 1086–1089 (2008).
23. A. Yildiz, M. Tomishige, R. D. Vale, P. R. Selvin, *Science* **303**, 676–678 (2004).
24. R. Schneider, T. Korten, W. J. Walter, S. Diez, *Biophys. J.* **108**, 2249–2257 (2015).
25. H. H. Sung *et al.*, *Dev. Cell* **15**, 866–876 (2008).
26. E. Gallaud *et al.*, *J. Cell Biol.* **204**, 1111–1121 (2014).

ACKNOWLEDGMENTS

We thank A. P. Carter and R. Tan for helpful discussions, L. Nocka for SEC-MALS experiments, B. LaFrance for MT image analysis advice, P. Grob, and J. Atherton for MT processing in RELION, D. Toso, J. Remis, and A. Chintangal for microscopy and computational support, the QB3 Macrolab for competent cell lines and TEV protease purification, the UC Berkeley Cell Culture Facility for providing the insect cells, the Cal-Cryo facility at UC Berkeley for EM imaging, and the Marconi100 for MD simulations.
Funding: This work was supported by grants from the National Institute of General Medical Sciences (GM094522 (A.Y.), GM123655-03 (L.F.), GM051487 (E.N.), GM127018 (E.N.), and the National Science Foundation (MCB-1617028 and MCB-1055017, A.Y.), PRACE (2019215144, MG), and Istanbul Technical University BAP (MGA-2021-42803, MG). E.N. is a Howard Hughes Medical Institute Investigator. **Author contributions:** L.F., L.E., Q.F., E.N., and A.Y. conceived the project and analyzed the data. L.F. and J.F. purified the proteins and performed single-molecule experiments. Q.F. and L.E. performed cryo-EM sample preparation, data collection, and analysis. Q.F., D.P.F, and F.D. performed Rosetta modeling. A.J. performed stepping measurements. M. Go. and M. Gu. performed MD simulations. T.H. collected and analyzed data for K490. K.C. created scientific illustrations. L.F., Q.F., L.E., M. Gur, E.N., and A.Y. wrote the manuscript, with further edits from all authors. **Competing interests:** The authors declare no competing interests. **Data and materials availability:** All data are available in data S1. Materials are available from A.Y. under a material agreement with the University of California, Berkeley. The coordinates for MAP7 bound to tubulin are available at the Protein Data Bank (PDB) with accession code 7SGS. All cryo-EM maps are available at the EMDB with accession codes EMD-25120 (FL MAP7), EMD-25119 (MAP7-MTBD and FL tau), EMD-25118 (MAP7 and kinesin), EMD-25117 (MAP7$^{83-134}$).

SUPPLEMENTARY MATERIALS

science.org/doi/10.1126/science.abf6154
Materials and Methods
Figs. S1 to S16
Tables S1 and S2
References (*27*–*57*)
MDAR Reproducibility Checklist
Movies S1 to S6
Data S1

View/request a protocol for this paper from *Bio-protocol*.

7 November 2020; resubmitted 28 July 2021
Accepted 8 December 2021
10.1126/science.abf6154